JOURNAL OF CATALYSIS 138, 101–114 (1992)

Hydrocarbon Formation from Methane by a Low-Temperature Two-Step Reaction Sequence

TIJS KOERTS, MARC J. A. G. DEELEN, AND RUTGER A. VAN SANTEN

Schuit Institute of Catalysis, Department of Inorganic Chemistry and Catalysis, Eindhoven University of Technology, PO Box 513, 5600 MB Eindhoven, The Netherlands

Received July 31, 1991; revised March 20, 1992

At atmospheric pressure thermodynamics limits direct conversion of methane to higher hydrocarbons to temperatures above 1200 K. Converting methane at lower temperatures requires at least two steps occurring under different conditions. This paper reports such a low-temperature conversion route toward ethane, propane, butane, and pentane without using oxygen. The overall reaction consists of two steps. Methane is dissociatively adsorbed on a Group VIII transition-metal catalyst at a temperature around 700 K, resulting in surface carbonaceous species and hydrogen. In the second step a particular carbonaceous intermediate is able to produce small alkanes upon hydrogenation around 373 K. The maximum yield to C_nH_{2n+2} ($n > 1$) obtained on a Ru catalyst is 13%.

INTRODUCTION

One of the intriguing problems in heterogeneous catalysis is the direct conversion of methane into other useful products. Methane activation is difficult because methane is a thermodynamically stable product with a noble gas-like configuration. The very strong tetrahedral C–H bonds [435 kJ/mol (*1*)] offer no functional groups, magnetic moments, or polar distortions to facilitate chemical attack. This makes methane less reactive than nearly all its conversion products. Especially in the selective oxidation of methane (*2*), this limits methane conversion to low conversions when a reasonable selectivity is to be achieved. Current practice of converting natural gas into higher hydrocarbons proceeds by the indirect route in which natural gas is first converted to synthesis gas at a high temperature (*3*). Subsequently hydrocarbons can be produced in a low-temperature exothermic process from synthesis gas, either by Fischer–Tropsch synthesis (*4, 5*) or via methanol and the MTG process (*6*). Direct methane conversion, like pyrolysis to acetylene and benzene (*7*), can only operate at temperatures above 1200 K (*8, 9*). At those very high temperatures graphite is much more stable than any hydrocarbon. Oxidative coupling of methane to ethene has been proposed as an alternative route (*10–14*). This reaction can result in C_{2+} hydrocarbon yields up to 25% when performed at temperatures around 1100 K. To increase the catalyst lifetime and the selectivity for C_{2+} hydrocarbons, there is interest for processes operating at lower reaction temperatures (*15, 16*).

A process for converting methane in several steps, but all occurring at lower temperatures, might have potential advantages. Of interest are recent experiments demonstrating that hydrocarbon formation is possible at low temperature, once methane is activated. Shelimov and Kazansky (*17*) activated methane on a molybdenum oxide catalyst by photochemisorption at pressures between 50 and 6000 Pa at room temperature. Upon desorption in vacuum, ethene, ethane, and propane were detected. Yang *et al.* (*18*) decomposed preadsorbed methane on a Ni(111) single crystal surface by a krypton bombardment at 47 K under ultrahigh-

0021-9517/92 $5.00

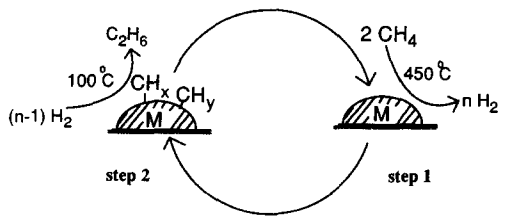

FIG. 1. Schematic presentation of the two-step route of methane conversion into ethane or higher hydrocarbons using transition-metal catalysts.

vacuum conditions ($P = 5 \times 10^{-6}$ Torr). They reported the selective desorption of benzene around 420 K from surface carbon fragments delivered by methane decomposition. Tanaka *et al.* (*19*) created surface CH_x fragments by dissociative methane adsorption around 700 K on cobalt catalyst. They succeeded in creating small amounts of ethene during hydrogenation and suggested that adsorbed CH_2 species are the precursor for ethene formation.

Here we report the formation of C_2 to C_6 alkanes from methane at atmospheric conditions in a two-step route in which methane is first thermally activated. At a temperature between 450 and 800 K methane is decomposed by a reduced Group VIII metal catalyst into hydrogen and adsorbed surface carbonaceous species (1). In a second reaction step a particular surface carbonaceous intermediate produces hydrocarbons upon hydrogenation at 300–400 K (2) (see Fig. 1):

$$2CH_4 + 6M \rightarrow 2M_3C + 4H_2 \quad (1)$$

$$2M_3C + 3H_2 \rightarrow C_2H_6 + 6M \quad (2)$$

$$2CH_4 \rightarrow C_2H_6 + H_2, \quad \Delta G(1000\ \text{K}) = 71.0\ \text{kJ/mol}, \quad (3)$$

where M = zero-valent transition metal.

Thermodynamics

The conversion of methane into ethane and hydrogen is thermodynamically not allowed in one reaction step (*20*), due to the positive change in Gibbs free energy. Therefore the introduction of oxidants like O_2 or Cl_2 has been used to convert the liberated hydrogen into H_2O or HCl. This lowers the change in Gibbs free energy to −121.6 and −130.6 kJ/mol, respectively. A different approach is to split the overall reaction (3) into two reaction steps occurring under different conditions. In such a two-step route the thermodynamic limitation can be circumvented as illustrated in Fig. 2. This is shown for the case that the reaction sequence involves formation of bulk cobalt carbide as intermediate.

The decomposition of methane on cobalt forming bulk cobalt carbide is endothermal while the change in entropy is negative. This reaction is only possible at temperatures above 632 K at standard concentrations and pressures (1 atm). The hydrogenation of bulk cobalt carbide to form ethane is exothermic and the change in entropy is negative. Therefore this reaction is favorable at low temperatures and can only occur below 347 K. There is no common temperature at which both reaction steps (1) and (2) can occur, so the temperature gap of 283 K is a thermodynamic stipulation. This temperature gap can be decreased by increasing the methane pressure during adsorption, increasing the hydrogen pressure in the second step, and by working at low conversion level.

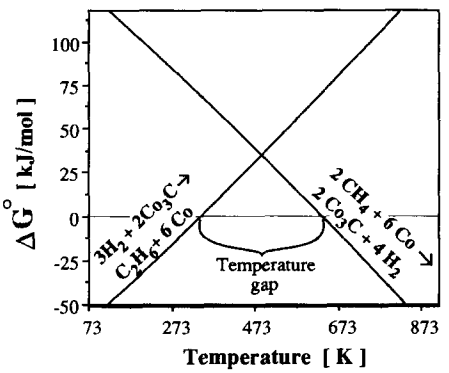

FIG. 2. Gibbs free energy as a function of the temperature for the decomposition of methane on cobalt and the hydrogenation of cobalt carbide to ethane.

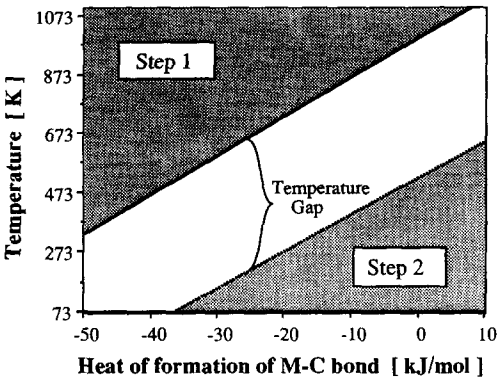

FIG. 3. Equilibrium temperatures for methane decomposition into surface carbides (dotted line) and hydrogenation of surface carbide to ethane (solid line) as a function of the metal–carbon bond strength. The shaded areas show the regions where reaction is possible. The equilibrium temperatures are calculated according to $T_{eq.} = \Delta H°/\Delta S°$. The temperature dependence of ΔH and ΔS are not taken into account.

The heat of formation of surface carbides is normally higher than that of bulk carbides. This will shift the lines in Fig. 2 to a lower temperature. The temperature at which the change in Gibbs free energy is negative depends on the heat of formation of the surface carbides. For a negative Gibbs free energy the reaction temperature should be above the equilibrium temperature for step (1), while it should be under the equlibrium temperature for step (2), as shown in Fig. 3.

The heat of adsorption of carbon atoms on the metal surface determines the working temperature areas for each metal catalyst and should be roughly between −60 and 20 kJ/mol. The heat of formation of surface carbide has been estimated by Shustorovich (*21*) for some transition metals. For iron the metal–carbon bond is −117 kJ/mol, which is too high (see Fig. 3); for copper the metal–carbon bond is 53 kJ/mol, which is too low. Nickel (4 kJ/mol) and cobalt (around −50 kJ/mol) have intermediate values and are in principle capable of performing the desired reaction sequence. Catalyst morphology and type of surface carbon as well as promoters can influence the metal–carbon bond strength and are therefore important parameters.

Instead of working in a temperature cycle it is possible to perform the reaction isothermally and work in a pressure swing, as recently indicated by Belgued *et al.* (*22*). These authors decomposed methane on a ruthenium and platinum catalyst into adsorbed surface CH_x fragments and hydrogen. Subsequently they hydrogenated those fragments in a pure hydrogen flow in which C_{2+} hydrocarbons were detected up to C_7. They were able to perform up to 90 cycles per hour. However, to overcome the ΔG of 71 kJ/mol, one is limited to very low product concentrations, as indicated by Fig. 4. The equilibrium pressures are given by Eqs. (4) and (5) for step (1) and step (2), respectively. From these the equilibrium conversions are calculated in a total pressure of 1 atm.

$$\frac{(p_{H_2})^2}{p_{CH_4}} = \exp\left[\frac{-\Delta G_{step(1)}}{RT}\right] \qquad (4)$$

$$\frac{p_{C_2H_6}}{(P_{H_2})^3} = \exp\left[\frac{-\Delta G_{step(2)}}{RT}\right]. \qquad (5)$$

ΔG is the change in Gibbs free energy for reaction step (1) in Eq. (4) and reaction step (2) in Eq. (5).

The equilibrium conversions in Fig. 4 are the maximum conversions reachable. This means that at 200°C, for example, the maximum methane conversion into graphite and hydrogen is 10^{-4} at 1 atm.

Dissociative Methane Chemisorption

Methane decomposition on transition-metal surfaces is an activated process and the activation energies found vary from 25 to 60 kJ/mol (*23–30*). These activation energies are quite low compared to those of, e.g., CO dissociation, while the temperature at which methane decomposition occurs with a useful yield is normally higher than that for CO dissociation, which has a higher activation energy. This is due to the low methane sticking coefficient. The mechanism of dissociative methane adsorption is

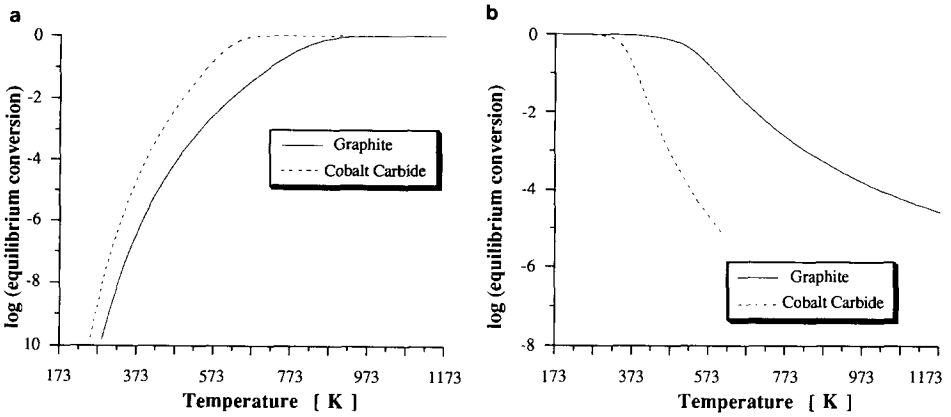

FIG. 4. The thermodynamic equilibrium conversions of reaction steps 1 and 2 in a total pressure of 1 atm as a function of the temperature. (a) Maximum fraction of methane converted into carbon and hydrogen. (b) Maximum fraction of hydrogen converted into ethane in the presence of carbon. Solid line, graphite as reaction intermediate; dotted line, bulk cobalt carbide as reaction intermediate.

not fully understood. From surface science studies on platinum (*31*) it appears that the surface temperature does not influence the methane sticking coefficient. Molecular beam studies show that high methane translation energies perpendicular to a metal surface enhance the methane dissociation probability substantially (*31, 32*). Also, internal vibrations enhance the methane sticking probability (*27, 28*). The mechanism for methane dissociation may involve quantum tunnelling of a proton as the rate-determining step (*31–33*). The large isotope effect for CD_4 is consistent with this mechanism (*34*). Beckerle *et al.* (*25*) proposed a mechanism which they called "chemistry with a hammer." In this mechanism, at low temperature adsorbed methane molecules are activated by collisions with other particles, which implies that the total pressure is important. Trevor *et al.* (*35*) studied methane decomposition on Pt metal clusters of different sizes and concluded that the methane decomposition rate is highest for clusters of two to five atoms. One metal atom is unable to dissociate CH_4, while in larger clusters (more than 5 atoms), the platinum atoms have higher coordination reducing the CH_4 decomposition rate. This agrees with results of Kuijpers *et al.* (*36*) on silica-supported nickel catalysts. They showed that methane decomposition is most efficient on small nickel particles.

EXPERIMENTAL

Catalysts

Transition-metal catalysts were prepared by incipient wetness impregnation of preshaped silica (Grace 332, surface area 300 m^2/g, mesh 100) with an aqueous solution of the metal nitrates or chlorides. The catalysts were dried at 110°C. The ruthenium catalyst was prepared from $RuCl_3$ and was treated after drying in a H_2/CO flow for 30 min at 250°C to increase its CO chemisorption capacity. The catalysts were characterized with transmission electron microscopy (TEM) and CO chemisorption.

Method

The reactions were performed in a microreactor which consisted of a quartz tube with an internal diameter of 10 mm. For each experiment 300 mg of the catalyst was placed in the reactor and was reduced *in situ* between 350 and 550°C in a diluted hydrogen flow. Methane decomposition was performed from a flow of 45 ml/min of diluted methane. Typically a pulse of 3 min of 0.5% methane in helium was given at 450°C. The

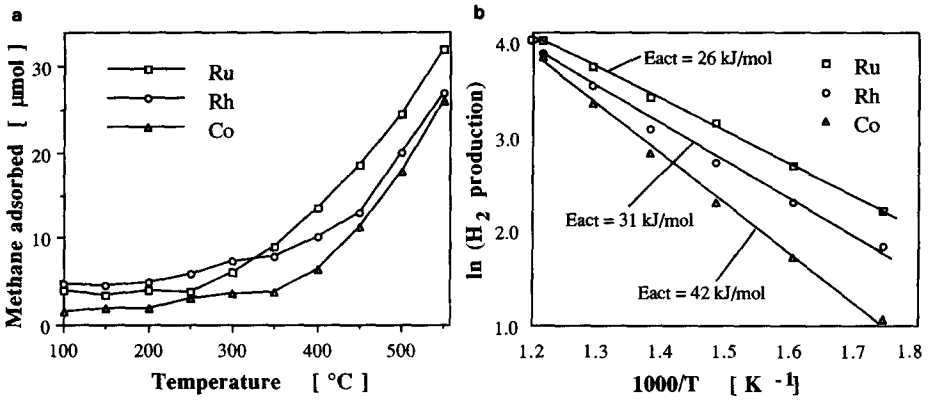

FIG. 5. (a) Fraction of methane adsorbed from a methane pulse of 3 min of 0.5% CH_4 in He as a function of the temperature on a 5% Ru, 3% Rh, and 10% Co catalyst. (b) Arrhenius plot of the hydrogen production.

methane flow contained no detectable amounts of ethane or other hydrocarbon impurities (less than 0.5 ppm). After methane decomposition, the catalyst was cooled in 100 s below 200°C to avoid "aging" of the surface carbon species. After cooling, surface carbon was hydrogenated to higher hydrocarbons in a flow of 22.4 ml/min of hydrogen at 100 kPa around 100°C. The surface carbon created from methane was characterized by a temperature-programmed surface reaction (TPSR) in a flow of 22.4 ml/min of 8% hydrogen in helium. Product analysis was performed on line with a quadrupole mass spectrometer (PGA 100 from Leybold) or with a gas chromatograph (CP 9000 from Chrompack) using a wide-bore column (plot q) of 25 m isothermal at 220°C at an inlet pressure of 200 kPa. With the GC system, every 20 s a sample could be taken to analyze the hydrocarbons C_1 to C_5.

RESULTS AND DISCUSSION

Methane Decomposition

The activity for methane decomposition into adsorbed surface carbonaceous species and hydrogen was studied for silica-supported ruthenium, rhodium, and cobalt catalyst, as a function of the temperature (see Fig. 5).

Already at 100°C a small amount of methane is adsorbed, as was also observed by Kuijpers *et al.* on nickel catalysts (*29*). At that low temperature no hydrogen desorption takes place. Above 300°C the sticking coefficient for methane chemisorption increases. The activation energies can be calculated from the temperature dependence of the fraction of methane adsorbed as well as from the amount hydrogen produced (Fig. 5b). These activation energies are 26 kJ/mol for ruthenium, 31 kJ/mol for rhodium, and 42 kJ/mol for cobalt in the temperature range 350–500°C. The ratio of hydrogen produced to methane adsorbed was 1.4 to 1.7 at temperatures between 400 and 500°C, indicating that the adsorbed carbon species contained still a little hydrogen or that not all the hydrogen atoms are desorbed from the catalyst. The methane decomposition rate appeared to be strongly dependent on the carbon coverage. Increasing the carbon coverage from 0 to 0.5 drastically decreased the rate of methane dissociation.

For the reduced transition metals studied the order of methane activation found is Co, Ru, Ni, Rh > Pt, Re, Ir > Pd, Cu, W, Fe, Mo. This corresponds with the order of activity for the methane–deuterium exchange reaction (*37, 38*). According to the unmodified bond order conservation principle (*39, 40, 21*) the activation energy for methane

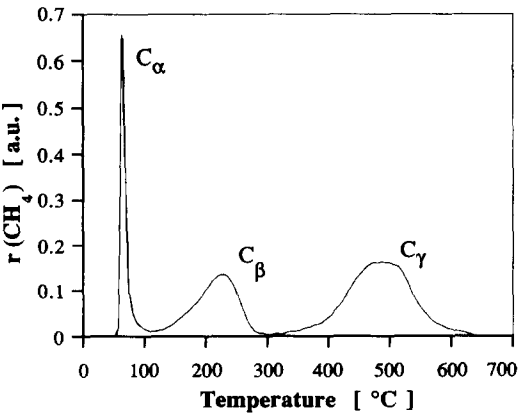

FIG. 6. Temperature-programmed hydrogenation of surface carbon created by methane decomposition on a 3 wt% silica-supported rhodium catalyst at 400°C.

decomposition is expected to be lower for metals with stronger *M*–C bonds. So for metals in the same row of the periodic table it is expected that the order for methane decomposition is Fe > Co > Ni > Cu. However, the results presented show an optimum at nickel and cobalt. This indicates that the activation energy also depends on the surface metal–metal bond strength as predicted by the *modified* bond order conservation principle (*41*).

Similarly as from dissociative CO adsorption (*42, 43*), CH_4 decomposition on reduced transition metals between 350 and 550°C results in different surface carbonaceous surface species. They are distinguished in their hydrogenation reactivity as is shown in the temperature-programmed surface reaction plot of Fig. 6.

A very reactive surface carbon species generated from CH_4 decomposition can be hydrogenated at 50°C or even below room temperature to methane. This surface carbon is called C_α. It has been identified by surface characterization techniques such as AES and SIMS on foils and single crystals as a carbidic type of carbon (*44–46, 32, 51*). Bell and co-workers (*47–50*) studied the nature of carbon types on a silica-supported ruthenium catalyst by NMR. They showed that this C_α carbon has only metal atoms in its first coordination shell (*47*). The presence of subsurface carbon cannot be excluded. Our quantum chemical calculations indicate that this carbidic carbon atom is adsorbed in hollow sites bonded to three or more surface metal atoms (*52, 53*). This carbidic carbon species consisting of C_α has been studied previously when generated from CO (*54–57*) and is responsible for higher hydrocarbon formation (*58, 59*). The mechanism of higher hydrocarbon formation from surface carbon from methane follows a Flory–Schulz–Anderson like distribution (see Fig. 10).

A less reactive surface carbon type (C_β) can be hydrogenated between 100 and 300°C. During the hydrogenation of C_β only traces of higher hydrocarbons up to C_6 were detected. The C_β species from CO as identified by Duncan *et al.* (*47, 60*) on ruthenium can be separated into C_{β_1} and C_{β_2}, which differ in their mobility. They showed that in this carbon phase C–C, M–C, and C–H interactions are present. Therefore, C_β is supposed to be an amorphous phase. After H_2/CO reaction Winslow and Bell (*49, 50*) were able to observe C–H stretch frequencies by FT–IR spectroscopy. We have noted with FT–IR spectroscopy that after methane adsorption at 450°C the C–H stretch frequencies totally disappeared from carbonaceous surface species adsorbed on a reduced ruthenium catalyst.

At temperatures above 400°C the poorly reactive C_γ reacts to produce only methane. This C_γ type surface carbon is a graphitic phase which consists of adsorbed connected six-rings. This carbon phase is probably located partially on the silica support as indicated by CO chemisorption measurements.

Because only the reactive C_α type carbon has reasonable selectivities for C_{2+} hydrocarbon formation upon hydrogenation, it is desirable to maximize its presence during methane decomposition. We have studied several parameters of CH_4 decomposition such as adsorption temperature, adsorption time, methane concentration, and aging time, which could influence the selectivities in the surface carbon formation. One of the

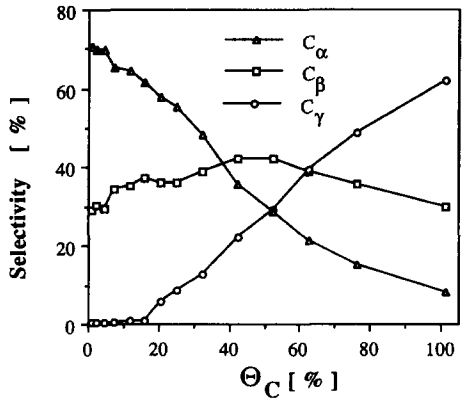

FIG. 7. Distribution of carbon types as a function of the carbon surface coverage on a 5% Ru/SiO_2 catalyst. Different carbon coverages were created by varying the methane adsorption time at 460°C.

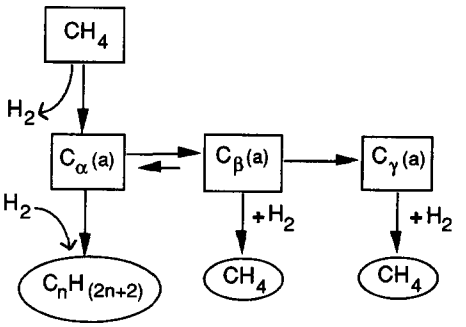

FIG. 8. Model for transformation of surface carbon types on transition metals.

parameters which appeared to be important is the carbon surface coverage remaining after methane decomposition (see Fig. 7).

Figure 7 shows that only at low carbon surface coverage is a high selectivity for reactive C_α type carbon obtained. The selective formation of reactive carbidic type carbon is related with the ability of the catalyst to form multiple-bonded surface carbon species (*51*). At coverages above 80% methane is mainly converted into an unreactive graphitic type of surface carbon. The distinction between C_β and C_γ was not sharp for all the catalysts. However, with increasing surface coverage, the carbon species always becomes less reactive.

From the methane decomposition experiments, a tentative reaction scheme can be formulated for the transformation of surface carbon to methane (see Fig. 8).

Methane is initially decomposed into carbidic C_α. This type of surface carbon can be transformed rapidly into C_β. C_β can be partially converted back into C_α. This model is in agreement with that of Bell and coworkers (*50, 47*) who showed that these carbon types can be in a dynamic equilibrium. C_β transforms slowly into the unreactive C_γ, a process called aging. This process is irreversible and its rate depends on the temperature, as found for nickel (*32*) and rhodium (*42*). It is not clear whether C_α can also be directly transformed into C_γ.

Hydrogenation Reaction of Surface Species to Alkanes

The second reaction step is the hydrogenation of surface carbon to produce C_{2+} hydrocarbons. Figure 9 shows the products formed as a function of the hydrogenation time after the reaction gas is switched from helium to hydrogen at 95°C.

By integrating the curves in Fig. 9 from time zero until time 4–10 min, the amount of hydrocarbon formed can be calculated.

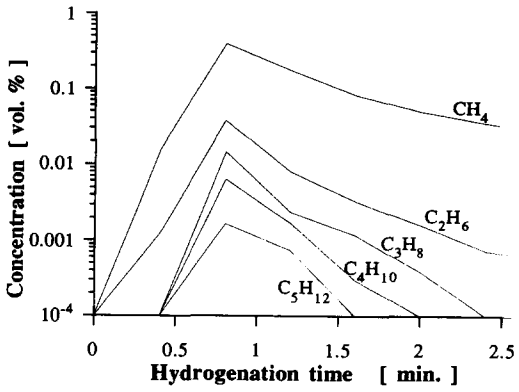

FIG. 9. Hydrogenation of surface carbon created from methane decomposition at 450°C, on a 10 wt% cobalt catalyst, as a function of the hydrogenation time. For butane and pentane the sum of the iso- and *n*-products is shown.

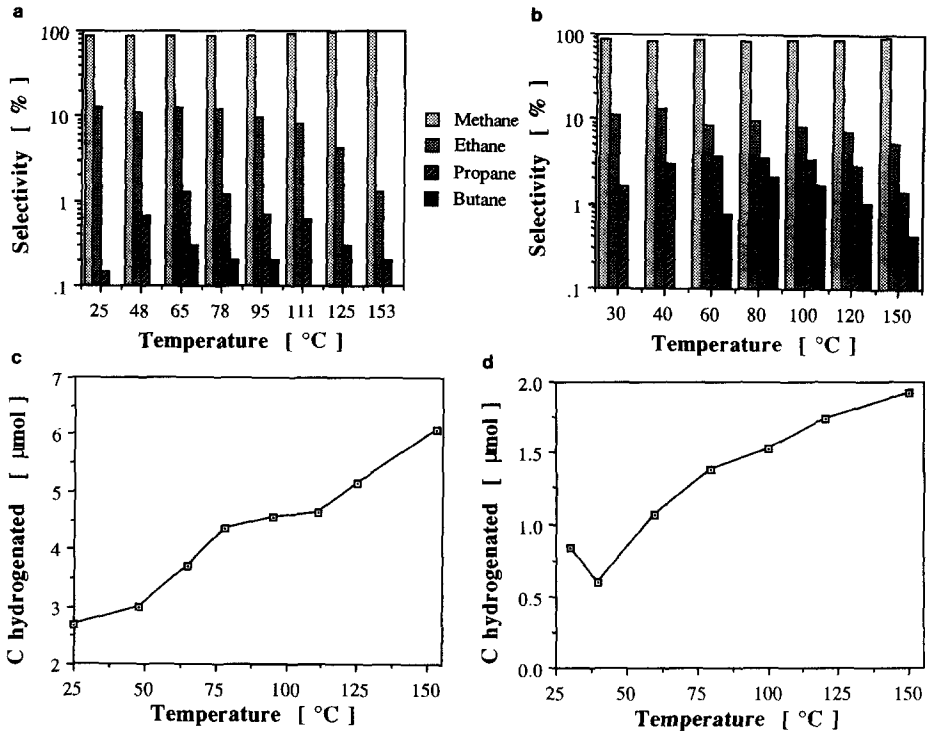

FIG. 10. Product distributions as a function of the hydrogenation temperature of surface carbon species, deposited from methane at 450°C, (a) 5% Ru/SiO_2. (b) 10% Co/SiO_2. Total amount of surface carbon that is hydrogenated; (c) Ru, (d) Co.

This leads to the product selectivity, which is given as carbon efficiency. The hydrocarbon selectivity follows a Flory–Schulz–Anderson type of distribution, indicating that adsorbed surface C_xH_y species can either be hydrogenated to $C_xH_{(2x+2)}$ or grow further to an adsorbed $C_{(x+1)}H_z$ species. The chain growth probability α determines the amount of C_{2+} hydrocarbons formed. In the plot of Fig. 9 the concentration of every subsequent hydrocarbon is about a factor of four lower, indicating that α is about 0.25.

As predicted by thermodynamics, the temperature at which C_α is hydrogenated is an important parameter, determining the selectivity for the formation of C_{2+} hydrocarbons.

Figure 10 shows the selectivities for C_{2+} hydrocarbon formation upon hydrogenation of surface carbon species generated from methane decomposition. At room temperature most of the surface carbon is hydrogenated to methane, 12% is hydrogenated to ethane, and only a trace of propane is formed. Increasing the temperature results in the hydrogenation of more surface carbon species (see Fig. 10c). On small metal particles different adsorption sites exist for carbon atoms, having slightly different metal–carbon interactions. The more strongly adsorbed carbon atoms are hydrogenated at higher temperatures and have higher probabilities for C–C bond formation versus methanation upon hydrogenation (*61, 62*). Therefore the selectivities for propane and butane increase when the temperature is raised above 25°C.

Figures 10c and 10d show that more surface carbon atoms are removed at temperatures above 130°C. Also at that temperature, unselective C_β is hydrogenated. This decreases the selectivity for C_{2+} hydrocar-

TABLE 1

Product Distribution of the Hydrogenation Reaction of Reactive Surface Carbon at 460°C on Reduced Silica-Supported Transition-Metal Catalysts

Catalyst	Particle size		Selectivities for hydrocarbons (%)				mmol[c]
	CO(*M*)[a]	nm[b]	CH_4	C_2H_6	C_3H_8	C_4H_{10}	
10% Co	2.2 (73)	8.5	79.6	11.3	6.11	2.92	8.0
5% Ru	35 (4.0)	5.5	80.5	15.8	2.69	1.00	7.10
10% Ni	13 (12)	9.2	89.3	7.3	1.89	1.40	16.8
3% Rh	55 (2.2)	2.2	95.8	4.12	0.09	0	3.4
	104 (0.8)	1.4	89.7	10.3	0	0	0.55
4% Pt	6.4 (24)	3.8	91.3	8.4	0.23	0	0.96
5% Re	30 (4.6)	3	98.4	1.3	0	0.29	0.95
4% Ir							

[a] Percentage chemisorption CO per metal atom. In brackets is the calculated particle size in nm assuming that every surface metal atom adsorbs 1 CO in a pyramid model.

[b] As measured with TEM.

[c] mmol surface carbon hydrogenated at 95°C.

bons. At temperatures above 180°C hydrogenolysis may transform some ethane back into methane, which explains why short contact times are favorable for high ethane selectivities. At temperatures above about 200°C the formation of higher hydrocarbons is thermodynamically forbidden and the surface carbon removed with hydrogen results in nearly only methane.

The optimum temperature for the formation of C_{2+} hydrocarbons depends on both the selectivity and the amount of surface carbonaceous intermediates hydrogenated. The optimum is around 95°C for ruthenium and cobalt catalyst. The highest C_{2+} hydrocarbon selectivities were obtained at short contact times and high hydrogen partial pressures, namely a residence time of 1.4 s at a p_{H_2} of 100 kPa. Higher hydrogen flows increase the C_{2+} hydrocarbon selectivity as also found by Belgued *et al.* (*22*). However, this is accompanied by a lower product concentration and by a less effective use of hydrogen.

Reduced transition-metal catalysts were compared in their ability to form C_{2+} hydrocarbons from methane. The catalysts were characterized by CO chemisorption and TEM. Methane adsorption occurred from a pulse of 3 min of 0.5% CH_4 in He at 460°C. The selectivity for the hydrocarbons formed during hydrogenation at 95°C as well as the amount of hydrogenated surface carbon at that temperature was measured (see Table 1).

Most of the butane was *n*-butane but isobutane also was detected. No alkenes were detected. On cobalt and ruthenium pentane formation also was observed. The metal particle size as measured with TEM and CO chemisorption does not agree for all catalysts, especially not for cobalt, rhenium, and nickel. This is ascribed to incomplete reduction of the metal. The cobalt and rhenium catalysts are especially difficult to reduce. In the metal/silica interface not fully reduced metal ions are probably present (*63*). A cobalt catalyst with a loading of 0.5% did not produce any higher hydrocarbons in the two-step procedure, and it did not chemisorb any CO. The real metal particle size is determined by TEM while the active reduced surface area is measured with CO chemisorption.

The ruthenium and cobalt catalysts are more selective toward higher hydrocarbon formation than rhodium, iridium, platinum, and nickel. Well-reduced iron, tungsten,

TABLE 2

Group VIII Transition-Metal Catalysts with their Chain Growth Probability α to Form C–C Bonds upon Hydrogenation at 95°C

Cr —	Mn —	Fe 0 0	Co 0.071 0.36	Ni 0.041 0.31	Cu 0 0
Mo 0 0	Tc —	Ru 0.098 0.18	Rh 0.022 0.015	Pd 0 0	Ag —
W 0 0	Re 0.046 0.018	Os —	Ir 0.007 0	Pt 0.057 0	Au —

Note. At the left, α_1 describing the chance for carbon–carbon bond formation of two adsorbed C_1 surface fragments; at the right α_2 describing the chance for subsequent insertion of CH_x intermediates in adsorbed hydrocarbon chains.

molybdenum, and copper catalysts were unsuitable for the stepwise transformation of methane into ethane. These results can be explained by analyzing the metal–carbon bond strength which determines the chance for C–C bond formation versus hydrogenation, as we recently suggested (*61, 62, 53*). This relation has been tested for Group VIII transition metals (see Table 2).

Going to the right in any one row of the periodic table, the metal *d*-valence electron band occupation increases and the metal–carbon bond strength decreases (*40, 41*). This is due to an enhanced occupation of the antibonding orbitals of the M–C orbitals (*64, 65, 53*). At increasing *d*-valence band occupation the chain propagation probability drops from 0.2 for cobalt to 0.09 for nickel and becomes zero for copper. However, for iron, with an even higher metal–carbon bond interaction, no formation of C_{2+} hydrocarbons occurs. No surface carbon that can be hydrogenated at the required low temperature is formed on the iron catalyst. This is shown in the temperature-programmed hydrogenation plot of Fig. 11.

Iron binds its surface carbon too strongly and no surface carbon is hydrogenated below 200°C. Thermodynamically, ethane formation is only possible at low hydrogenation temperatures (see Figs. 2 and 3) and therefore iron catalysts are not suitable for this reaction sequence, although they are known as good Fischer–Tropsch catalysts, where they are active as a carbidic phase (*68*). Only around 250°C were some parts per million of ethane detected.

Thus for transition metals of rows three and four of the periodic table, the formation of ethane from surface carbon behaves according to the Sabatier principle. Ruthe-

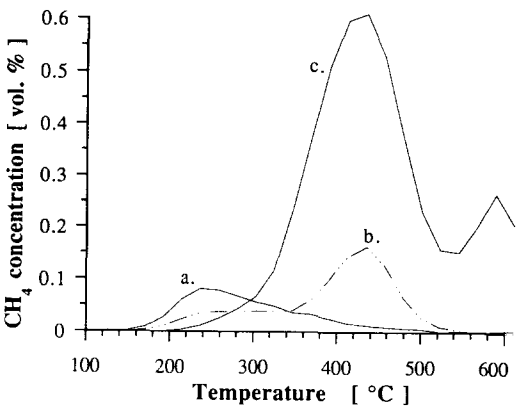

FIG. 11. Hydrogenation of surface carbon from methane on a 10% Fe/SiO_2 catalyst with different surface carbon loadings, 300 mg of the catalyst containing, respectively, 0.55 μmol surface carbon (a) (methane concentration multiplied by 10), 8.9 μmol carbon (b), and 53.6 μmol surface carbon (c). Different carbon surface coverages were created by varying the methane adsorption time at 500°C.

nium and cobalt are found to be optimum in their metal–carbon bond strength. In the fifth row, platinum is an exception. The optimum in the fifth row is expected at rhenium due to a M–C bond strength similar to that of ruthenium and cobalt.

Both alkali and other metal oxide promoters have been shown to influence the metal–carbon bond strength (*66, 67*) and can therefore be expected to play an important role in changing the selectivity. We have tested the influence of basic (MgO) and acidic (V_2O_5) catalyst supports. These supports do not improve the catalytic performance of the metal particles. The results obtained on alumina (Ketjen, CK-300) were a little better than those obtained on silica.

Carbon–carbon bond formation is a structure-sensitive reaction similar to the opposite reaction of hydrogenolysis. Therefore, larger metal particles are expected to show a higher carbon–carbon bond formation. The selectivity for C_{2+} hydrocarbons was increased when a ruthenium catalyst was sintered, indicating that larger particles are indeed favorable for carbon–carbon bond formation.

Yield and Heat and Mass Balance

The overall yield of the formation of C_{2+} hydrocarbons from methane is controlled by the conversion of methane during its decomposition, the selectivity for C_α surface carbon formation, and the chain growth probability upon hydrogenation. These parameters are a function of the "carbon" surface coverage as shown in Figs. 12 a–12d.

The rate of carbon–carbon coupling is low at very low carbon surface coverages (Fig. 12c). Raising the carbon surface coverage, the chain growth probability increases to 0.15 at a monolayer carbon coverage. However, at surface coverages above 20% the selectivity for the formation of C_α carbon drops (Fig. 12b). Therefore, the optimum overall yield for the formation of C_{2+} hydrocarbons from methane is reached at a surface coverage of only 0.18. The maximum yield for C_{2+} hydrocarbon from methane is 13% which is a true yield because the methane conversion during adsorption is 100%, under the conditions used, until a carbon surface coverage of 25% is reached (Fig. 12a).

In the reaction resulting in a yield of 13%, a pulse of 4.57 μmol methane was given from a flow of 40 ml/min with 0.28% CH_4 at 450°C, over 300 mg of the reduced catalyst. This resulted in surface carbon (2.66 μmol C_α, 1.61 μmol C_β, and 0.04 μmol C_γ), 7.6 μmol gas-phase hydrogen, and 0.26 μmol CO_2. Upon the subsequent reaction with hydrogen at 100 kPa at 95°C, 2.66 μmol surface carbon reacted, from which 21% was incorporated into C_{2+} hydrocarbons.

The exact heat effects of the two reaction steps depend on the heat of adsorption of the surface carbon fragments. We have tried to estimate the heat of adsorption of a carbon atom on ruthenium from data of Shustorovich (*39, 40*) and from a comparison of Fig. 3 with our experimental data: $\Delta H_{Ru-C} = -20 \pm 10$ kJ/mol. ΔH for methane decomposition into surface carbon and hydrogen at 100 kPa, at 450°C, is equal to 59 kJ/mol. The hydrogenation of ruthenium surface carbide to ethane at 100 kPa is accompanied by a ΔH of -29 kJ per mol ethane formed. The high-temperature step is entropy-driven and consumes heat, while the low-temperature step is enthalpy-driven. The transport of heat from a high temperature [step (1)] to a low temperature (step (2)], is unfavorable from an industrial point of view. However, it forms the driving force for the overall conversion of methane to higher alkanes, which is thermodynamically impossible in one step.

The overall yield of 13% is of the same order as that obtained with high-temperature pyrolysis and selective oxidation. Oxidative coupling can result in a yield that is nearly twice as high.

CONCLUSIONS

Thermodynamic temperature limitations for methane conversion to higher hydrocar-

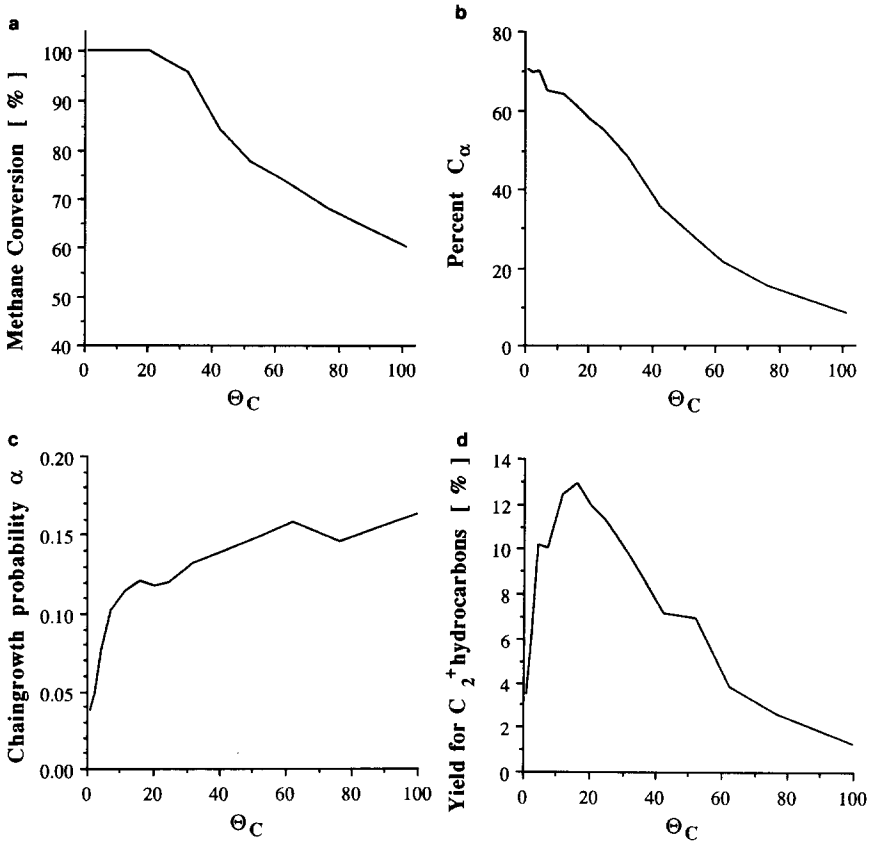

FIG. 12. Methane decomposition at 450°C followed by hydrogenation at 95°C on a 5% Ru/SiO_2 catalyst. Different carbon surface coverages were created by varying the adsorption time. (a) Methane conversion. (b) Percentage of C_α type carbon. (c) Chain growth probability. (d) Yield for the formation of C_2+ hydrocarbons. All are as a function of the carbon surface coverage.

bons can be circumvented using a two-step process. We have indicated the theoretical and practical conditions for such a new conversion route of methane conversion to small alkanes and hydrogen without the use of oxidants. In such a process carbon–carbon bond formation occurs upon hydrogenation from a specific surface carbon intermediate, generated by thermal decomposition of methane. The selective formation of this carbidic reaction intermediate is favored by low carbon surface coverages. The carbon–carbon bond formation mechanism is similar to the process responsible for chain growth in the Fischer–Tropsch reaction. The metal–carbon bond strength in this process is important and is optimum for the cobalt and ruthenium catalysts used.

The maximum temperature needed for the presented methane conversion route (about 400–450°C) is much lower than that of conventional routes.

REFERENCES

1. Golden, D. M., and Benson, S. W., *Chem. Rev.* **69,** 125 (1969).
2. Pitchai, R., and Klier, K., *Catal. Rev. Sci. Eng.* **28,** 13 (1986).
3. Rostrup-Nielsen, J. R., *in* "Catalysis, Science and Technology" J. R. Anderson and M. Boudart, Eds.), Vol. 5. Springer, Berlin, 1984.
4. Vannice, M. A., *Catal. Rev. Sci. Eng.* **14,** 153 (1976).
5. Pichler, H., *Adv. Catal.* **4,** 271 (1952).

6. Chang, C. D., *in* "Natural Gas Conversion" (A, Holmen, K-I. Jens, and S. Kolboe, Eds.). Elsevier, Amsterdam, 1991.
7. van der Zwet, G. P., Hendriks, P. A. J. M., and van Santen, R. A., *Catal. Today* **4,** 365 (1989).
8. Kirk, R. E., and Othmer, D. F., *in* "Encyclopedia of Chemical Technology" (M. Grayson and D. Eckroth, Eds.), 3rd ed. Vol. 1, p. 180. Wiley–Interscience, New York, 1984.
9. Geerts, J. W. M. H., Ph.D. thesis, p. 35, Eindhoven, 1990.
10. Keller, G. E., and Bhasin, M. M., *J. Catal.* **73,** 9 (1982).
11. Hinsen, W., and Baerns, M., *Chem. Ztg.* **107,** 223 (1983).
12. Ito, T., Wang, J-X., Lin, C. H., and Lunsford, J. H., *J. Am. Chem. Soc.* **107,** 5062 (1985).
13. Sofranko, J. A., Leonard, J. J., and Jones, C. A., *J. Catal.* **103,** 302 (1987).
14. Otsuka, K., Jinno, K. and Morikawa, A., *Chem. Lett.* **499** (1985).
15. Heinemann, H., Somorjai, G. A., Pereira, P., and Lee, S. H., *Catal. Lett.* **6,** 255 (1990).
16. Roos, J. A., Bakker, A. G., Bosch, H., van Ommen, J. G., and Ross, J. R. H., *Catal. Today.* **1,** 133 (1978).
17. Shelimov, B. N., and Kazansky, V. B., *J. Chem. Soc. Faraday Trans. I* **83,** 2381 (1976).
18. Yang, Q. Y., Johnson, A. D., Maynard, K. J., and Ceyer, S. T., *J. Am. Chem. Soc.* **111,** 8748 (1989).
19. Tanaka, K-I., Yaegashi, I., and Aomura, K., *J. Chem. Soc. Chem. Commun.* 938 (1982).
20. Amenomiya, Y., Goledzinowski, M., Birss, V., Galuszka, J., and Sanger, A. R., *Catal. Rev. Sci. Eng.* **32**(3), 63 (1990).
21. Shustorovich, E., *Adv. Catal.* **37,** 101 (1990).
22. Belgued, M., Amariglio, H., Pareja, P., Amariglio, A., and Saint-Juste, J., *Nature* **352,** 789 (1991).
23. Bond, G. C., *in* "Catalysis by Metals" Academic Press, New York, 1962.
24. Lee, M. B., Yang, Q. Y., Tand, S. L., and Ceyer, S. T., *J. Chem. Phys.* **85,** 1693 (1986).
25. Beckerle, J. D., Yang, Q. Y., Johnson, A. D., and Ceyer, S. T., *J. Chem. Phys.* **86,** 7236 (1987).
26. Tavares, M. T., Bernardo, C. A., Alstrup, I., and Rostrup-Nielson, J. R., *J. Catal.***100,** 545 (1986).
27. Brass, S. G., and Ehrlich, G., *Surf. Sci.* **191,** L819 (1987).
28. Brass, S. G., and Ehrlich, G., *Surf. Sci.* **187,** 21 (1987).
29. Kuijpers, E. G. M., Jansen, J. W., van Dillen, A. J., and Geus, J. W., *J. Catal.* **72,** 75 (1981).
30. Sun, Y. K., and Weinberg, W. H., *J. Vac. Sci. Technol. A* **8,** 2445 (1990).
31. Schoofs, G. R., Arumainayagam, C. R., McMaster, M. C., and Madix, R. J., *Surf. Sci.* **215,** 1 (1989).
32. Sault, A. G., and Goodman, D. W., *Adv. Chem. Phys.* **76,** 153 (1989).
33. Rettner, C. T., Pfnür, H. E., and Auerbach, D. J., *Phys. Rev. Lett.* **54,** 2716 (1985).
34. Kay, B. D., and Coltrin, M. E., *Surf. Sci.* **198,** L375 (1988).
35. Trevor, D. J., Cox, D. M., and Kaldor, A., *J. Am. Chem. Soc.* **112,** 3742 (1990).
36. Kuijpers, E. G. M., Breedijk, A. K., van der Wal, W. J. J., and Geus, J. W., *J. Catal.* **72,** 210 (1981).
37. Frennet, A., *Catal. Rev. Sci. Eng.* **10,** 37 (1974).
38. Kemball, C., *Adv. Catal.* **11,** 223 (1959).
39. Shustorovich, E., *Surf. Sci.* **176,** L863 (1986).
40. Shustorovich, E., *Catal. Lett.* **7,** 107 (1990).
41. Van Santen, R. A., *Recl. Trav. Chim. Pays Bas.* **109,** 59 (1990).
42. Solymosi, F., and Erdöhelyi, A., *Surf. Sci.* **110,** L630 (1983).
43. McCarty, J. G., and Wise, H., *J. Catal.* **57,** 406 (1979).
44. Niemantsverdriet, J. W., and van Langeveld, A. D., *Catalysis,* 769 (1987).
45. Van Langeveld, A. D., and Niemantsverdriet, J. W., *Surf. Interface Anal.* **9,** 215 (1986).
46. Goodman, D. W., Kelley, R. D., Madey, T. E., and Yates, J. T., Jr., *J. Catal.* **63,** 226 (1980).
47. Duncan, T. M., Winslow, P., and Bell, A. T., *J. Catal.* **93,** 1 (1985).
48. Duncan, T. M., Winslow, P., and Bell, A. T., *Chem. Phys. Lett.* **102,** 163 (1983).
49. Winslow, P., and Bell, A. T., *J. Catal.* **91,** 142 (1985).
50. Winslow, P., and Bell, A. T., *J. Catal.* **86,** 158 (1984).
51. Somorjai, G. A., and van Hove, M. A., *Prog. Surf. Sci.* **30,** 201 (1989).
52. De Koster, A., and van Santen, R. A., *J. Catal.***127,** 141 (1991).
53. Koerts, T., and van Santen, R. A., *J. Mol. Catal.* **70,** 119 (1991).
54. Mori, T., Miyamoto, A., Takahashi, N., Fukagaya, M., Hattori, T., and Murakami, Y., *J. Phys. Chem.* **90,** 5197 (1986).
55. Araki, M., and Ponec, V., *J. Catal.* **44,** 439 (1976).
56. Koerts, T., Welters, W. J. J., and van Santen, R. A., *J. Catal.* in press.
57. Rabo, J. A., Risch, A. P., and Poutsma, M. L., *J. Catal.* **53,** 295 (1978).
58. Biloen, P., and Sachtler, W. M. H., *Adv. Catal.* **30,** 165 (1981).
59. Winslow, P., and Bell, A. T., *J. Catal.* **94,** 385 (1985).
60. Duncan, T. M., Reimer, J. A., Winslow, P., and Bell, A. T., *J. Catal.* **95,** 305 (1985).
61. Koerts, T., and van Santen, R. A., *Catal. Lett.* **6,** 49 (1990).
62. van Santen, R. A., De Koster, A., and Koerts, T., *Catal. Lett.* **7,** 1 (1990).
63. van der Grift, C. J. G., Ph.D. thesis, Utrecht, 1990.

64. Feibelman, P. J., *Phys. Rev. B* **26,** 5347 (1982).
65. Darling, G. R., Joyner, R. W., and Pendry, J. B., *in* "Structure and Reactivity of Surfaces" (C. Morterra, A. Zecchina, and G. Costa, Eds.), p. 335. Elsevier, Amsterdam (1989).
66. Ichikawa, M., Fukushima, T., and Shikakura, K., *in* "Proceedings, 8th International Congress on Catalysis, Berlin, 1984," Vol. II, p. 69. Dechema, Frankfurt-am-Main, 1984.
67. Mross, W. D., *Catal. Rev.* Sci. Eng. **25,** 591 (1983).
68. Dry, M. E., *in* "Applied Industrial Catalysis" (B. E. Leach, Ed.) Vol. 2, p. 167. Academic Press, New York, 1983.